Plasma Spraying of Ceramic Particles in Argon-Hydrogen D.C. Plasma Jets: Modeling and Measurements of Particles in Flight Correlation with Thermophysical Properties of Sprayed Layers

P. FAUCHAIS, M. VARDELLE, A. VARDELLE, and J.F. COUDERT

The behavior of alumina or stabilized zirconia particles in flight in Ar-H_2 d.c. plasma jets (up to 40 kW) has been studied. Measurement of the temperature distributions in the plasma jets (by emission spectroscopy) has shown the importance of the electrodes and arc chamber designs on the length and diameter of the jets. The important cooling effect of the surrounding air has also been shown, and the parameters controlling it have been studied. Modeling of the momentum, mass, and heat transfers between plasma and particles as well as measurements of the trajectory, velocity, surface temperature distributions, and particle evaporation have enabled us to determine the influence of the different parameters, such as size and injection velocity distributions, particle morphology, *etc.*, on the particle molten state upon impact. These calculations and measurements on the particles in flight have been correlated to some physical properties of deposits.

I. INTRODUCTION

THE plasma spraying process consists of introducing solid particles into a d.c. plasma jet in order to accelerate and, if possible, melt these particles to form a coating with the splats, resulting in a lamellar structure. Almost any material that can be melted without evaporating or decomposing (with at least 300 K difference between melting and evaporation or decomposition temperatures) can be used to form the coating. The production of dense, high-strength deposits requires[1–8] that:

(1) a large fraction (if not the whole) of the injected powder particles be heated to a molten state before they impinge on the substrate or the previously deposited layers;
(2) besides being in a molten state, the particles should also have sufficient velocities to be able to spread out and flow into the irregularities of the previously deposited layers;
(3) a strong interparticle or particle-substrate bond should be formed; and
(4) a good control of the residual stresses' distribution should be obtained with an appropriate cooling of the deposit during spraying.

Points (1) and (2) and, to a lesser extent, point (3) depend strongly on the momentum and heat transfers between the plasma jet and the injected particles. Much work, especially in the laboratory, has been devoted to studying these transfers theoretically and experimentally. The aim of this paper is to point out our present knowledge in the field, particularly for ceramic powders sprayed with Ar-H_2 plasma jets at atmospheric pressure. This will be illustrated with recent calculations or measurements performed in the lab and correlated, if possible, to the thermomechanical properties of the resulting deposits. Thus, the following will be presented successively:

(1) models;
(2) measurement techniques;
(3) plasma jet temperature distributions; and
(4) velocity, trajectory, and surface temperature distributions of particles upon impact.

II. MODELS

A. *Plasma Flows*

Important advances were made through the more or less routine application of transport equations[9,10,11] to plasma flows, especially recently, taking into account the turbulent mixing with the surrounding gas, using temperature-dependent physical properties and more rigorous equations satisfying the overall balances, as well as radially-dependent torch exit profiles. The last point is particularly important, because as actually no one is able to model the plasma at the electrodes, the exit profiles must be given; and the jet temperature and velocity distributions are very dependent on these exit profiles that have to be measured, at least for the temperature ones.[9,10,11]

B. *Particles*

1. *Individual particles*

Although there are certain similarities between ordinary fluids and thermal plasmas, heat and momentum

P. FAUCHAIS, Professor, M. VARDELLE, A. VARDELLE, and J.F. COUDERT, Associate Professors, are with the Laboratoire Céramiques Nouvelles (UA 320), University of Limoges, 123 Rue Albert Thomas, 87060 Limoges Cedex, France.

This paper is based on a presentation made in the T.B. King Memorial Symposium on "Physical Chemistry in Metals Processing" presented at the Annual Meeting of The Metallurgical Society, Denver, CO, February, 1987, under the auspices of the Physical Chemistry Committee and the PTD/ISS.

transfers between plasma and particles are much more complex, due to the presence of charged particles, chemical reactions, and steep gradients, which are characteristic of thermal plasmas. However, according to the reviews of Pfender,[12] Chen,[13] and A. Vardelle,[14] for given temperature and velocity distributions in the plasma jet, the main parameters controlling the trajectory, velocity, and temperature history of individual particles, assumed to be spherical, are the following:

1) corrections to the drag and Nusselt coefficients to account for the steep temperature gradients;
(2) noncontinuum effects (even at atmospheric pressure);
(3) propagation phenomenon inside the particle; and
(4) evaporation.

To illustrate the difficulty in deducing very precise results from the theories, A. Vardelle has recently calculated[14] the behavior of various ceramic particles injected into a 29 kW Ar-H_2 plasma jet whose temperature and velocity distributions have been measured previously.[15,16] Figure 1 shows the trajectories and velocities of an alumina particle 20 μm in diameter injected into this plasma jet. These particles were injected into the plasma with the ideal injection velocity (corresponding to a mean deviation of 3 deg with the torch axis) calculated for a particle-neglecting rarefaction of evaporation effects. For a given particle size and injection velocity, the differences between trajectories result from the corrections for the steep temperature gradients between the plasma (up to 13,000 K) and the surface temperature of the particle (3500 K at best). For these corrections, two methods have been used: mean integrated thermal properties[17] or correction factors proposed either by Lewis and Gauvin[18] or by Lee and Pfender.[19] Similar differences are observed whatever the particle size may be (at least below 100 μm, for which the calculations were performed). Figure 2 indicates that at atmospheric pressure, the noncontinuum effect in this spraying Ar-H_2 plasma jet is not negligible, even for 60 μm particles. This is due to the high mean free paths of atoms and molecules at these temperatures. Figure 3, for a 20 μm diameter particle, shows both influences of vapor and noncontinuum corrections. It is worth noticing that the vaporization has been taken into account only by calculating the energy necessary to heat up the vapor, and no corrections have been made for the transport properties modification due to the presence of vapor. Presently, to our knowledge, no transport properties calculations have been made for complex plasma mixtures with oxide vapors due to the lack of data for interaction potentials. Finally, when Ar-H_2 plasmas (where the heat transfer coefficient reaches values between 20,000

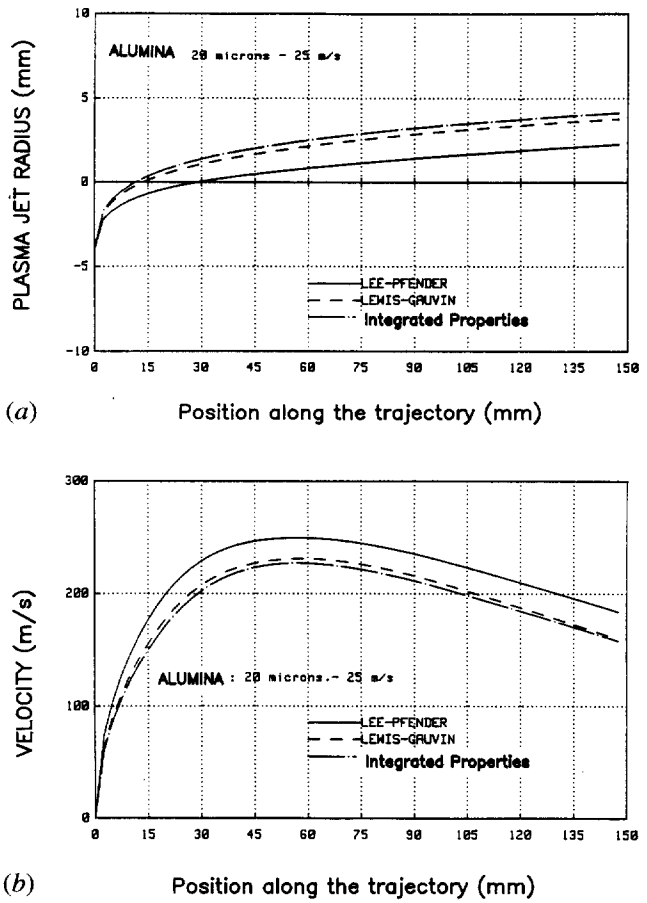

Fig. 1—(*a*) The calculated trajectory and (*b*) velocity evolution along the trajectory of an alumina particle 20 μm in diameter injected into an argon-hydrogen d.c. plasma jet (29 kW, 75 l/min Ar, 15 l/min H_2). Calculations were performed for three different theories accounting for the steep gradients between particle and plasma.[14]

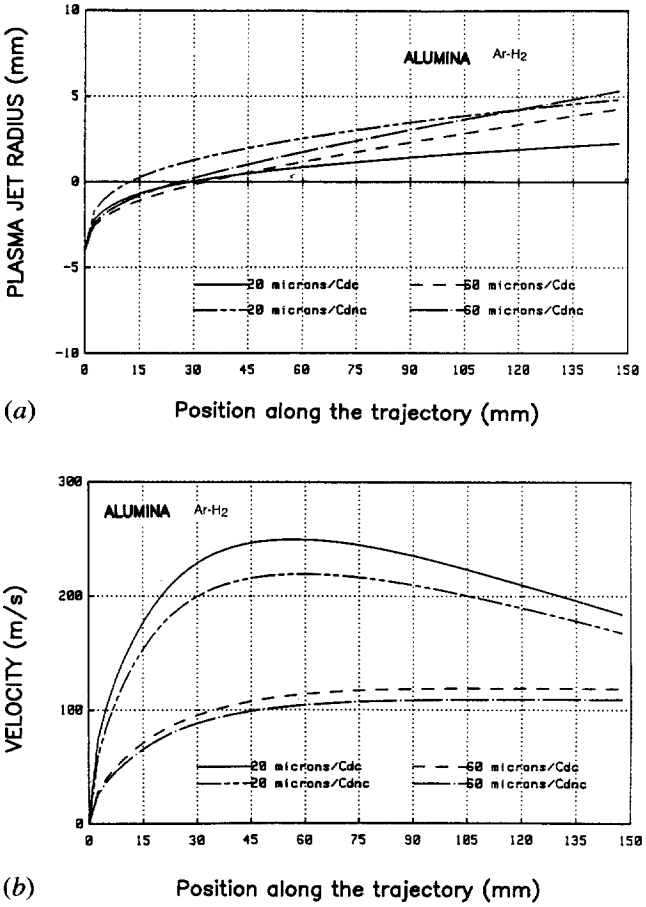

Fig. 2—(*a*) The calculated trajectory and (*b*) velocity evolution along the trajectory of alumina particles 20 and 60 μm in diameter, respectively, injected into an argon-hydrogen plasma. Calculations were performed taking into account noncontinuum effects.[14] Cdc drag coefficient with continuum theory and Cdnc in noncontinuum theory.

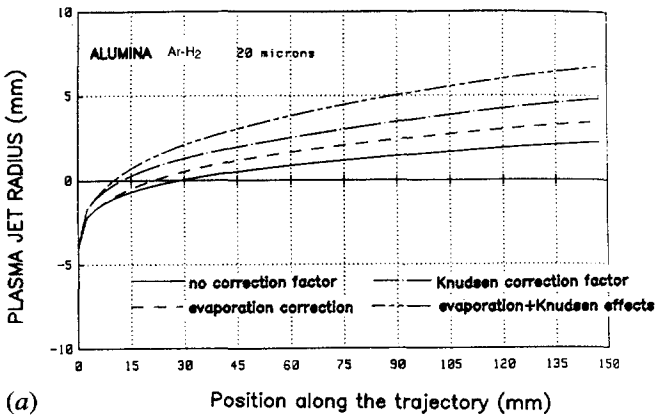

(*a*)

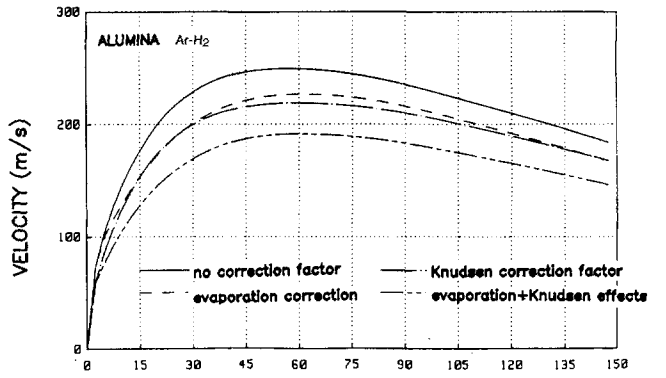

(*b*)

Fig. 3—(*a*) The calculated trajectory and (*b*) velocity evolution along the trajectory of alumina particles (20 μm in diameter) injected into an argon-hydrogen plasma. Calculations were performed taking into account noncontinuum and evaporation effects.[14]

and 100,000 $W/m^2 \cdot K$[14]) are used to spray ceramic particles, a heat transfer phenomenon occurs inside the particles. This is illustrated in Figure 4 for a 100 μm diameter alumina particle injected with a velocity of 2 m/s into a 29 kW N_2-H_2 plasma.[20] The evaporation and noncontinuum effects have not been taken into account, and the mean integrated thermal conductivity method has been used. In Figure 4, plotted against time (*i.e.*, particle position along its trajectory divided by its velocity), is the plasma temperature seen by the particle (right axis) and the surface temperature, center temperature, and temperature of the particle calculated with no heat propagation phenomenon (left axis), respectively. The curve calculated for an infinite thermal conductivity, *i.e.*, a uniform particle temperature, represents relatively well the mean temperature of the particle. It can be seen that the difference between the center and surface temperatures is tremendous (>1500 K), and the surface of the particle reaches melting temperature even though its center is still cold. Previous calculations[17] for infinite plasmas have shown that this phenomenon occurs almost whatever the size the particle may be, and this explains the tremendous evaporation of such ceramic particles, especially the small ones, after a few millimeter trajectories. With this heat propagation phenomenon, the distance between torch nozzle exit and substrate must be such that the center of the particle reaches melting temperature. As can be seen in Figure 4, such a location (or time in the figure) does not correspond to the maximum surface temperature of the particle (about 1.1 ms), because center temperature is still rising. Finally, it must be remembered that for plasma spraying, the total length of the plasma jet is not infinite, as will be explained in Section IV, and the residence time of the particle is limited. Thus, the particle size is of some importance for its complete melting. For example,[14] an alumina particle immersed in an infinite Ar-H_2 plasma (17 vol pct H_2) at 10,000 K will melt in 0.03 seconds if its diameter is 20 μm against 0.7 seconds for a 100 μm particle and 0.15 seconds for a 50 μm particle.

The particle melting in a real plasma jet will depend both on the residence time of the particle and on the heat transfer from the plasma. Figure 5 represents the temperature evolution of the heat transfer coefficient h for an alumina particle 50 μm in diameter with a relative velocity of 50 m/s and a surface temperature of 1000 K in the Ar-H_2 plasma, with h calculated[14] using different theories to account for the steep gradients. The discrepancies observed (especially the peaks at 6000 K) are difficult to explain, due to the number of parameters used to calculate the corrections. However, as the gas properties for the corrections giving the peaks are calculated at the film temperature, the dissociation temperature of H_2 plays an important role with the corresponding maxima of C_p and K. Whatever the "good" correction may be, Figure 5 shows that the heat transfer coefficients are nearly constants for temperatures higher than 8000 K, *i.e.*, in the plasma core where heating occurs. Thus, the heating will be mainly controlled by the particle velocity, depending on the drag coefficient C_D and on the relative velocity plasma particle. Figure 6 shows the evolution of C_D with temperature for the same conditions as those given in Figure 5. The highest values are obtained with the highest temperatures. For the same conditions, the drag coefficient is almost multiplied by a factor of 2 when the particle diameter decreases from 50 to 20 μm, whatever the temperature may be. Thus, the

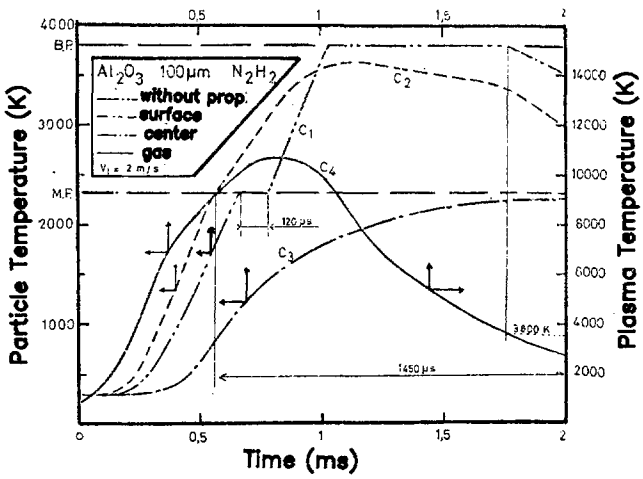

Fig. 4—The evolution with residence time (particle position/particle velocity) of the surface and center temperatures of an alumina particle (100 μm in diameter) of the particle temperature (infinite thermal conductivity is considered to be uniform) and of the plasma temperature seen by the particle along its trajectory in a 29 kW N_2-H_2 plasma.[20]

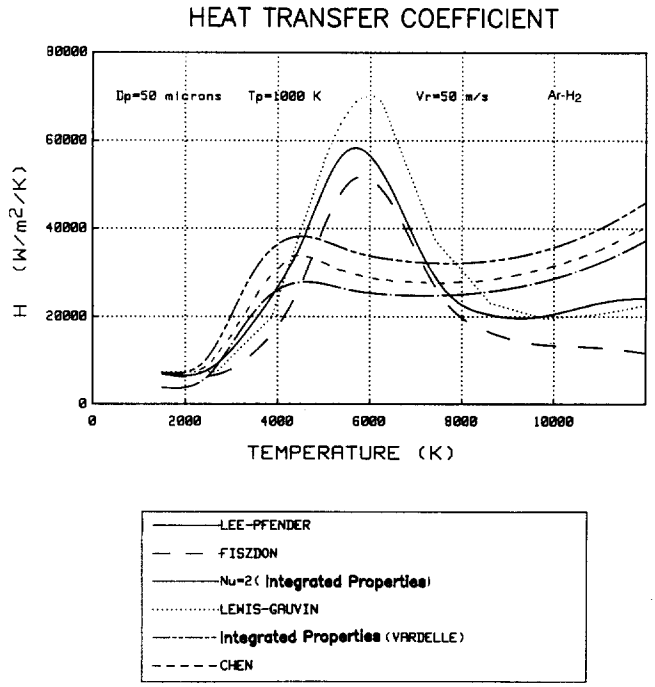

Fig. 5—The evolution with temperature of the heat transfer coefficient in an Ar-H_2 plasma (17 vol pct H_2) for an alumina particle 50 μm in diameter with a surface temperature of 1000 K and a relative plasma-particle velocity of 50 m/s. This coefficient has been calculated[14] according to different theories.

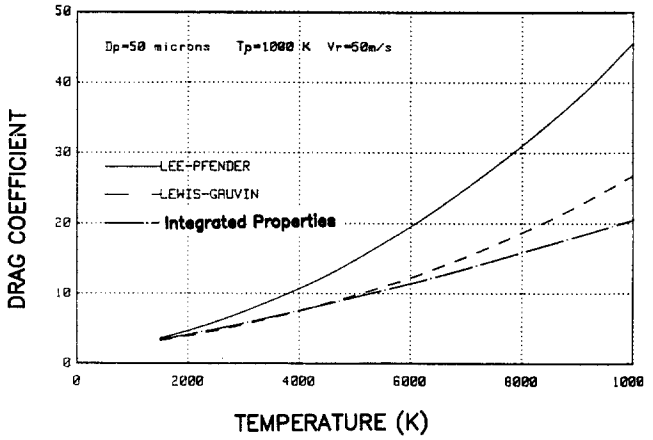

Fig. 6—The evolution with temperature of the drag coefficient in an Ar-H_2 plasma (17 vol pct H_2) for an alumina particle 50 μm in diameter with a surface temperature of 1000 K and a relative plasma-particle velocity of 50 m/s. This coefficient has been calculated[14] according to different theories.

smallest particles will have the shortest residence times. For example,[21] the maximum velocity reached by an 18 μm diameter alumina particle is only twice that reached by a 46 μm particle in the same plasma jet. As the melting times are in a ratio of 5 to 6, even with a lower residence time, the melting of the 46 μm particle will not be as good as that of the 18 μm particles. However, the heat transfer to the smallest particles is also reduced by the noncontinuum and evaporation effects.

All these calculations show how reliable experimental data are necessary to check the heat and momentum transfer expressions and to clarify the effects of various complicated factors within the boundary layers and on the particle surface.

2. *Particle size and injection velocity distributions*

The injection velocity is of primary importance for the particle trajectory, velocity, and surface temperature, as illustrated in Figure 7 for a 100 μm diameter alumina particle injected into a 29 kW N_2-H_2 plasma. However, in practice, particles with a given size distribution are injected in the plasma jet with the help of a carrier gas. This injection mode corresponds to an injection velocity distribution, even for monosize particles, and finally the trajectory distribution results from the product of the injection velocity and size distributions.[14,16] The injection velocity (to obtain an ideal trajectory) is, of course, the

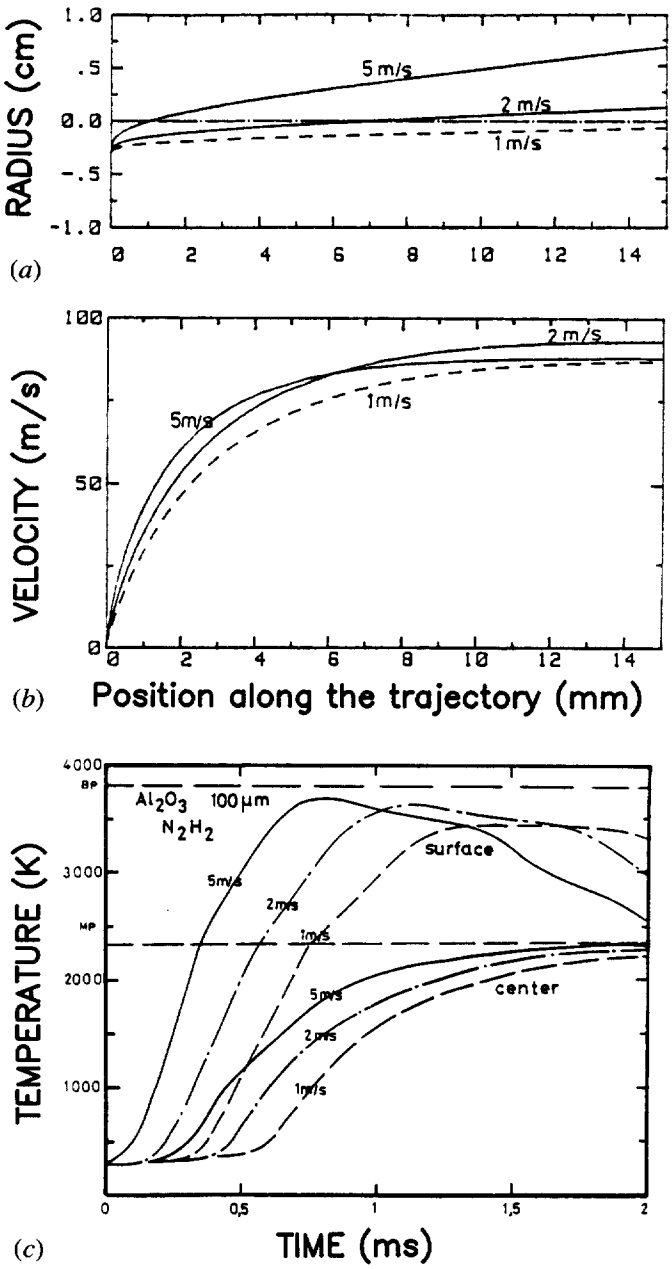

Fig. 7—The influence of the injection velocity on (*a*) trajectory, (*b*) velocity, and (*c*) surface temperature along trajectory of alumina particles (100 μm in diameter) injected into a 29 kW N_2-H_2 plasma.[14]

highest for the smallest particles (for example, 25 m/s for 18 μm Al_2O_3 particles against 2 m/s for 100 μm ones). For a given injector, the injection velocity distribution is the broadest for the highest carrier gas flowrate (corresponding to the highest mean gas velocity); small particles, even with a narrow size distribution, will have a broad injection velocity distribution, whereas big particles, even with a broad size distribution, will have a narrow injection velocity distribution. Thus, the trajectory distribution inside the plasma jet (for example, see the results presented in Reference 16) is rather broad whatever the powder nature, density, and size distribution may be, and the complete statistical analysis of the measurements to compare with models is an essential part of the experiment.

C. *Plasma-Particles Interactions*

In the models presented, it has been assumed that there is no coupling between the gas and particulate phases; *i.e.*, the particle density is low enough to avoid plasma jet cooling. However, as shown by Pfender,[12] the cooling of the plasma occurs as soon as the ratio of particle mass flowrate to plasma gas mass flowrate is higher than 0.2. For the 29 kW Ar-H_2 plasma jet considered, this is the case as soon as more than 15 g/min of alumina powder is injected, as illustrated by the recent calculations of Proulx *et al.*[22] for this plasma. This is shown in Figure 8, representing the evolution of the centerline temperature and velocity profiles for different alumina powder loadings. With strong loading, the plasma jet is practically cooled in a few centimeters from the jet exit, and, of course, the heat transfer to the particles is strongly reduced. This can be correlated to the deposits obtained with alumina particles (−45 + 10 μm) injected radially into the 29 kW Ar-H_2 plasma jet (see Section III–C for the spraying conditions). The open porosity (which depends on the particle temperature and velocity upon impact) is almost constant (5 pct) up to 900 g/h and starts to increase for higher powder flowrates. Moreover, heat transfer to the particles is reduced when small particles are sprayed. In fact, it is not really a loading effect but a reduction of the heat transferred to the particles due to the important vapor cloud surrounding each particle.[14,23] This is illustrated by the results obtained when spraying small (−12 + 5 μm) zirconia particles stabilized with calcia (7.6 wt pct) with an Ar-H_2 plasma at a power level of 40 kW.[24] Up to a powder feed rate of 0.5 kg/h, the open porosity P_v is constant (10 pct) as well as the sprayed layer density (ρ = 5430 kg/m^3), but it decreases for higher feed rates (for example, P_v = 11 pct, = 5.37 at 0.95 kg/h). Then it remains almost constant up to 1.6 kg/h (the cooling effect of the plasma by the loading decreases the particle evaporation). This is also confirmed by the measurements of the monoclinic phase content in the as-sprayed deposits. As calcia evaporates faster than zirconia, as shown by our measurements,[23] the percentage of the monoclinic phase in the as-sprayed deposit increases with the power level but decreases with the powder flowrate. At 8 g/min, 25 pct of the monoclinic phase is measured against 5 pct at 25 g/h. For bigger particles (−40 + 22 μm), the porosity increase starts at powder flowrates higher than 0.85 kg/h.

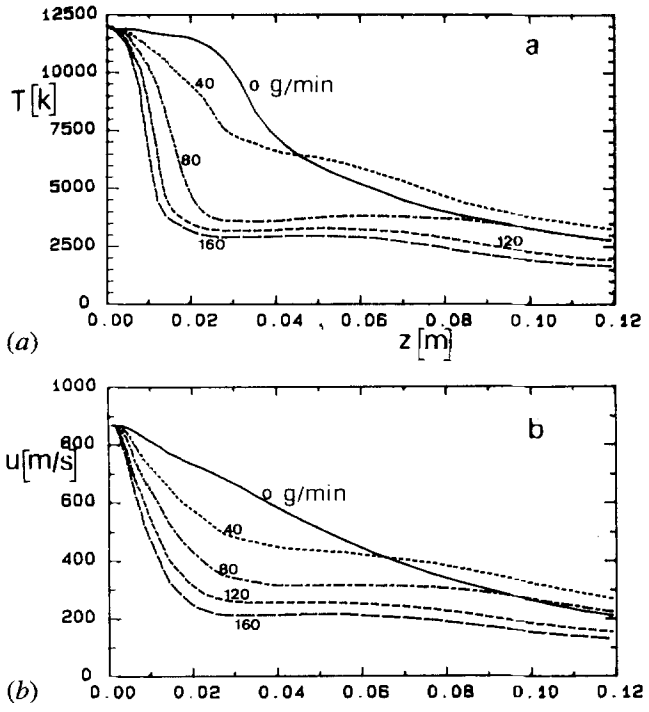

Fig. 8—(*a*) The axial temperature and (*b*) velocity profiles of an argon-hydrogen (17 vol pct) plasma jet with alumina particles injected radially with different flowrates.[22]

III. MEASUREMENTS AND EXPERIMENTAL CONDITIONS

A. *Plasma Jet Temperature*

The plasma jet temperature has been measured in the frame of a CLTE (complete local thermal equilibrium) assumption by emission spectroscopy of atomic argon lines. The image of the plasma jet is formed on the entrance slit of the monochromator, and a 2 D OMA (optical multichannel analyzer) detector is located at the position of the photographic plate.[25,26] This device provides the only means to sample simultaneously (*i.e.*, in a few milliseconds) all the data relative to the spectra at different positions of plasma jet cross-section. The stored line intensities, including Abel's inversion, are then treated numerically. Most of the measurements have been performed by using the emission coefficient of the ArI line at 826.4 nm. The error due to the composition modification by the pumping of the surrounding air has been evaluated to be less than 8 pct in the fringes of the jet (in comparison with temperatures deduced from the atomic lines ratio).

B. *Particles in Flight*

The flux density, the velocity, and the surface temperature distributions of the solid particles in flight in the plasma jet have been measured simultaneously with the experimental setup already described by M. Vardelle.[16,27] The particle density was measured in different cross-sections of the plasma jet by counting, during a given time, the pulses resulting from the light scattered by the particles passing through the focused point of a laser beam.

The mean particle trajectory is obtained by moving the measurement volume (or, more precisely, by moving the plasma jet relative to the measurement volume) along two orthogonal directions and determining the corresponding radial distributions. The position of the two maxima corresponds to the mean trajectory in the plasma jet "slice" considered.

The particle velocity distribution was measured by laser dual focus velocimetry (L2F) or laser doppler anemometry (LDA) with interferential arrangement. The particle surface temperature distribution was determined by two-color pyrometry (for details see Vardelle[23] and Mishin[27]).

Of course, all these measurements are statistical ones, and the values obtained for the parameter X are mean values for n particles passing through the corresponding measurement volume:

$$\bar{X} = \frac{1}{n}\sum_{i=1}^{n} X_i$$

Emission or absorption spectroscopy was used to measure the concentration of the metallic species (resulting from the ceramic evaporation) in the plasma jet[28] and emission spectroscopy to determine the size and temperature distribution in the vapor cloud surrounding one particle in flight.[29]

C. *Spraying Conditions*

A homemade d.c. plasma torch was used to spray the powders of alumina and stabilized zirconia used for the measurements in flight and the coating properties analysis. The thoriated tungsten cathode was the stick type (with an 8 mm diameter rod), and the nozzle was convergent followed by a cylindrical tube 8 mm in diameter and 18 mm long. The powder was injected radially either inside the nozzle, 2 mm upstream of its exit, or outside the nozzle, 2 mm downstream. The inside diameter of the injector was 1.6 mm, and the carrier gas, pure argon. The plasma jet was a mixture of Ar and H_2 with a total flowrate either of 60 l/min (25 vol pct H_2) or of 90 l/min (17 vol pct H_2). Ar-H_2 mixtures have been chosen because of the longer plasma jets obtained compared with pure argon ones[23,30] but also for the much better heat transfer to the particles.[14,17,23,30,31] The power level of the torch was varied between 15 and 40 kW (by adjusting the arc current between 200 and 600 A). All the deposits were sprayed on disk substrates (ϕ = 25 mm) disposed all around the ring of a rotating disk (ϕ = 200 mm) whose axis was perpendicular to that of the plasma torch. In all the experiments, the rotation speed was kept constant as well as the velocity of the torch (in the direction parallel to that of the substrate). The deposits were cooled during spraying by air jets blown at their surface, and the plasma jet was prevented from heating the coating and substrate by an air barrier.[32] The coating surface temperature, measured by IR Thermography, was kept below 120 °C during spraying. Spraying distance has been adjusted in order to have a melting of the particles as complete as possible (see the discussion of heat propagation phenomenon in Section II–B–I). Open porosity of the deposit is, for example, a good parameter for adjusting the spraying distance. When the particle is not completely molten or has started to solidify again, the porosity increases. This is illustrated in Figure 9 representing, for the 90 l/min Ar-H_2 plasma, the open porosity evolution *vs* spraying distance for three zirconia powders stabilized with 8 wt pct yttria. For the two small particle distributions (−25 + 10 μm) and (−12 + 5 μm), the optimum distance is d = 75 mm. For smaller values, the particle is not completely molten even if the surface temperature is decreasing (see Section V), and for higher values, the particle is cooling down. It is worth noting that there is almost no difference between 28 and 32 kW (see Section IV). For the biggest particles (−75 + 20 μm), there is almost no minimum. This is probably due to the lower temperature of the bigger particles, with an incomplete melting of their central part. Such measurements have been confirmed with alumina deposits for which an incompletely melted particle crystallizes in the α phase and not in γ. For example, with the Ar-H_2 plasma jet, the optimum spraying distance for the −21 + 15 μm alumina particles at 29 kW is 75 mm. At this distance, the porosity P is 9 pct and the ratio $R = \gamma/(\alpha + \gamma)$ = 6 pct, at a distance of 90 mm P = 12 pct and R = 9 pct against P = 13 pct and R = 10 pct for 65 mm. It is worth noting that the distance of 75 mm corresponds to a zone where the surface temperature is decreasing (see Section V–B).

IV. PLASMA JETS TEMPERATURE DISTRIBUTIONS

The plasma jet temperature isocontours result from the following parameters:[33]

(1) the nozzle and arc chamber designs and shapes;
(2) the arc current I;
(3) the total gas flowrate m° and nature, especially for the Ar-H_2 mixture, the H_2 vol pct; and
(4) the mixing with the surrounding gas which increases with the arc current and total gas flowrate.[34]

What makes matters complex[33] is the plasma gas distribution between the hot core of the plasma (where temperatures are higher than about 6000 K) and the cold (below 3000 K) gas flowing close to the nozzle wall. The percentage of hot gas (neglecting the demixing

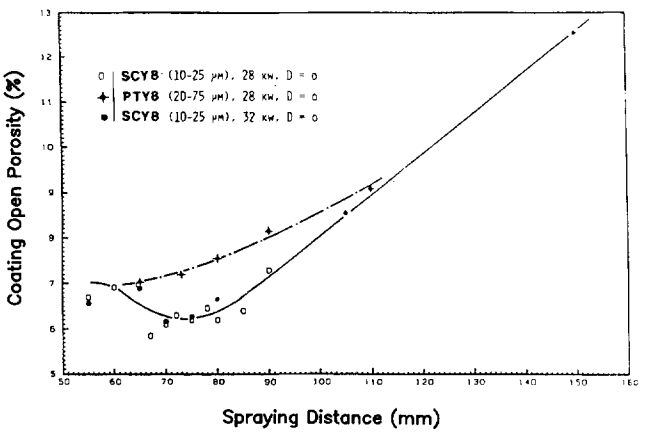

Fig. 9—The evolution of the open porosity with spraying distance for three zirconia powders stabilized with yttria (8 wt pct) with different size distributions.[24]

problems) depends on the hot plasma expansion from the cathode tip controlled (besides the designs, shapes, and dimensions of the cathode, arc chamber, and nozzle) by the arc current, total gas flowrate, and hydrogen percentage. A few rules, however, have been established[30,33] for the plasma column diameter which increases with I, decreases with m°, and decreases with H_2 pct. However, as soon as the jet exits from the nozzle, the fast pumping of the surrounding air, with oxygen dissociation at 4000 K, cools it down very fast. For example, Figure 10 shows the evolution along the axis of the plasma gas percentage for our Ar-H_2 29 kW plasma jet; 30 mm downstream of the nozzle exit, this percentage is only 30 pct. This pumping effect, as shown by the measurements of Brossa and Pfender,[34] increases with arc current and plasma gas flowrate. This is illustrated by our measurements shown in Figures 11 and 12. Figures 11(a) and (b) show, respectively, a comparison of the isotherm of the two plasma jets used for spraying (see Section III–C). Figure 11(a) corresponds to the 75 l/min Ar + 15 l/min H_2 plasma and Figure 11(b) to the 45 l/min Ar + 15 l/min H_2 one, both for the same arc current and almost the same torch efficiency (60 pct for the highest flowrate and 56 pct for the lowest). The measurements have been started 3 mm downstream of the nozzle exit, and both figures show the fast expansion of the plasma jet as soon as it flows in free atmosphere; for example, the 9000 K isotherm diameter 3 mm downstream of the nozzle exit is larger than the nozzle exit diameter. The total increase of the flowrate results in a rise of the length of the hottest isotherms ($T > 12{,}000$ K), when for the coldest ones, due to the increase of the surrounding air pumping, it results in a decrease of their

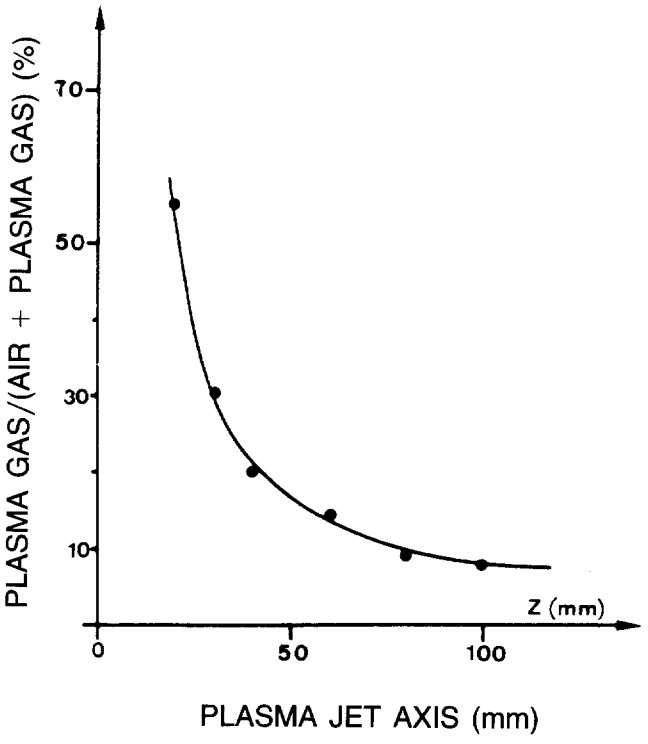

Fig. 10—The evolution along the plasma jet axis of the percentage of plasma gas (compared to its mixture with air) for the Ar-H_2 29 kW plasma jet.[14]

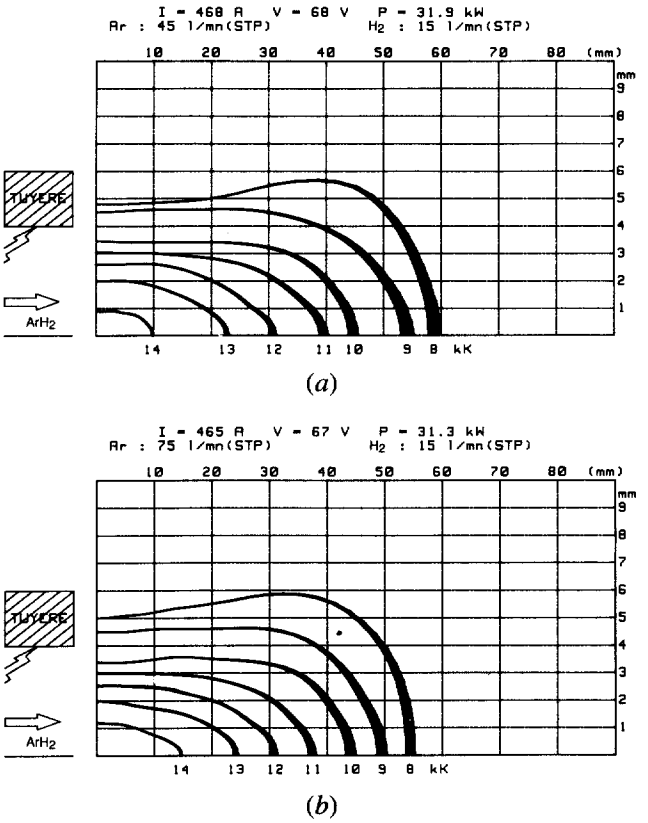

Fig. 11—The plasma jet temperature distributions for argon-hydrogen plasma jets flowing in air with the flowrates of (*a*) D_{Ar} = 75 l/min, D_{H_2} = 15 l/min and (*b*) D_{Ar} = 45 l/min, D_{H_2} 15 l/min, respectively.

length. The importance of this air pumping (resulting in a fast cooling of the jet) is well illustrated in Figure 12 where, for almost the same conditions (except a slight difference in arc current for the 90 l/min plasma, resulting in a power level of 33.2 kW against 31.9 in Figure 11), the plasma jets are flowing in an argon atmosphere. The lengthening of the hottest isotherms ($T > 11{,}000$ K) is even more marked, and due to the less cooling efficiency of argon (compared to air), the isotherms up to 9000 K have almost similar lengths. The most spectacular effect of argon is the drastic increase of the jet diameter; for example, 43 mm downstream of the nozzle exit, the 9000 K isotherm for the 90 l/min plasma is 58 mm in an argon atmosphere compared to 36 mm in air.

Due to this complex air pumping, which increases with arc current, the increase of the plasma jet length with power level (for a given total gas flowrate) is not as important as the power level ratio. For example, when increasing the power level of the 60 l/min plasma from 23.5 to 33.5 kW (*i.e.*, a ratio of 1.43), the length ratios of the 12,000 and 9000 K isotherms are, respectively, 1.23 and 1.12. However, the diameter of the isotherms increases with the higher current,[33] and the particle penetration in the plasma jet is easier (see Section V–A).

It is worth noting the fast expansion of the "cold" isotherms ($T < 10{,}000$ K) whose diameter, 3 mm

ISOTHERMS FROM 727.2 nm ATOMIC LINE OF ArI IN A CONTROLLED ATMOSPHERE CHAMBER

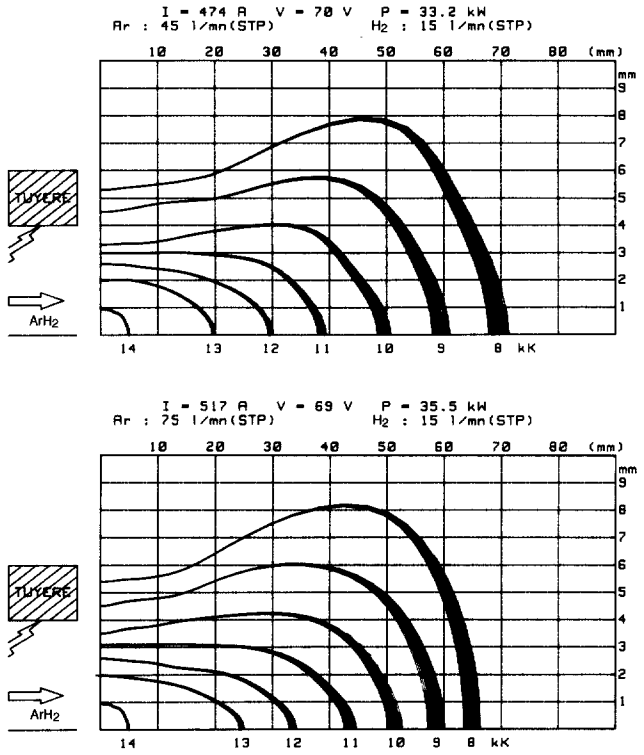

Fig. 12—The plasma jet temperature distributions for the same plasmas as in Fig. 11 but flowing in argon atmosphere.

downstream of the nozzle exit, is bigger than the nozzle diameter. This is probably due to the turbulent mixing with the surrounding atmosphere. It is also important to emphasize that this expansion is more important in an argon atmosphere, because oxygen dissociation at about 4000 K cools down the plasma jet fringes very quickly.

V. PARTICLE VELOCITY, TRAJECTORY, AND SURFACE TEMPERATURE DISTRIBUTIONS

A. *Particle Injection*

As already emphasized (see Section II–B–2), the injection velocity plays an important role in the trajectory distribution. This is illustrated in Figures 13 and 14. Figures 13(a) and 14(a) represent the size distribution of two different alumina powders: $-21 + 15$ μm and $-90 + 45$ μm, respectively, when Figures 13(b) and 14(b) represent the measured velocity distributions at the injector exit.[23] Of course, the largest particles are injected with a low mean injection velocity corresponding to a carrier gas flowrate of 2.5 l/min, while the smallest ones are injected with a high mean injection velocity corresponding to a carrier gas flowrate of 7.5 l/min. It is quite obvious that injection velocity distribution of the small particles is very broad even if the size distribution is very narrow. The broadness of the injection velocity is related mainly to the particle size and, of course, mean injection velocity, rather than to their size distribution. For example,[14] compared to the $-90 + 45$ μm particles (mean size of 63 μm) injected with an argon carrier gas flowrate of 2.5 l/min (v_{inj} = 12.7 m/s), $-70 + 50$ μm particles injected with the same carrier gas flowrate (v_{inj} = 13.8 m/s) have almost the same injection velocity distribution. The net result is a broader particle trajectory distribution for the smallest alumina particles ($-21 + 15$ μm) than for the biggest ones ($-90 + 45$ μm), as illustrated in Figures 15(a) and (b). This figure represents the normalized particle flux density in a "slice" of the plasma jet 75 mm downstream of the nozzle exit, *i.e.*, where the substrate is normally disposed to spray the coatings. Such trajectory distributions will result in different heat treatments, as illustrated in the next section.

B. *Particle Trajectory, Velocity, and Surface Temperature Distributions*

The particle trajectory, velocity, and surface temperature distributions have been measured in different plasma

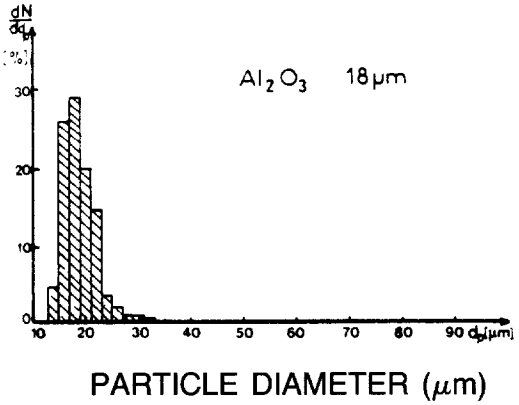

(*a*)

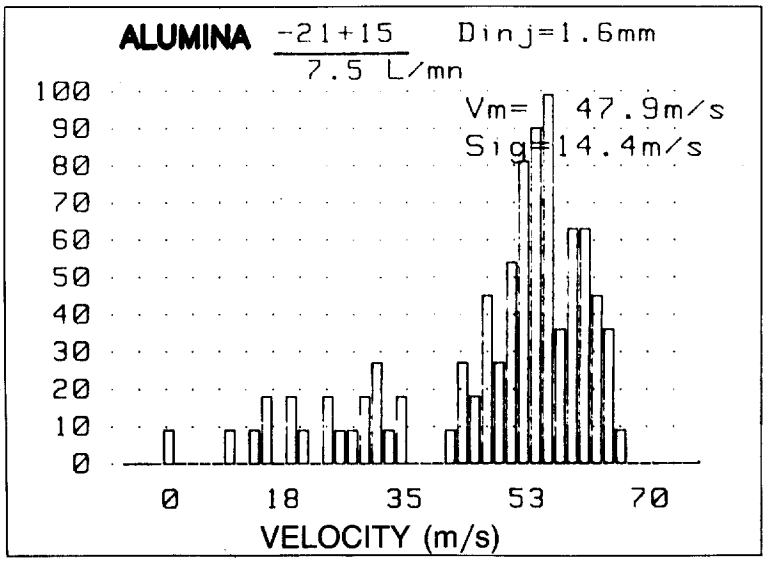

(*b*)

Fig. 13—Alumina particles ($-21 + 18$ μm): (*a*) size distribution and (*b*) injection velocity distribution (carrier gas flowrate: 7.5 l/min).

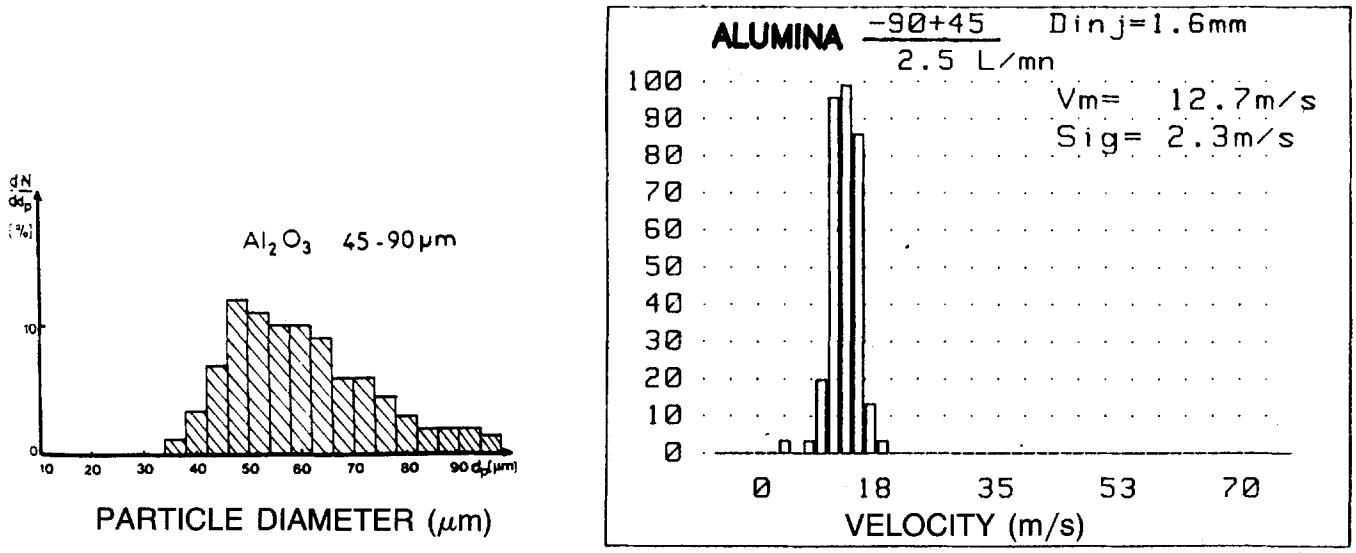

(*a*) (*b*)

Fig. 14—Alumina particles (−90 + 45 μm): (*a*) size distribution and (*b*) injection velocity distribution (carrier gas flowrate: 2.5 l/min).

jet "slices." Of course, all the presented results correspond to particle size distributions which have been injected with the optimum injection velocity for the mean size of the distribution. This means that especially with particle distribution containing a tail of small particles, the smallest particles will not penetrate into the hot core of the jet and travel in its fringes where they can be melted but with drastically reduced evaporation.

1. *Influence of the particle size*

The smaller the particles, the higher their acceleration (as well as their deceleration), as illustrated in Figure 16 (velocity evolution along the mean trajectory) for two size distributions ((−21 + 15 μm) and (−52 + 40 μm)) of fused alumina particles injected into the 29 kW Ar-H_2 plasma jet (45 l/min Ar-15 l/min H_2). A similar influence of the particle inertia is shown in Figure 17, representing the evolution of the surface temperature T_s of these two particle distributions. It must be remembered that no T_s measurement is possible within the first 50 mm downstream of the nozzle exit where the plasma emission is a few orders of magnitude higher than that of the particles. For the 18 μm particles, T_s has reached its maximum in the plasma core itself, when for the 46 μm particles, the maximum of T_s is obtained at a distance of about 70 mm. However, the surface temperature of the 18 μm particles decreases much faster than that of the 46 μm. Moreover, even along the trajectory, the velocity and surface temperature distributions are rather broad within the measurement volume. Figure 18 shows

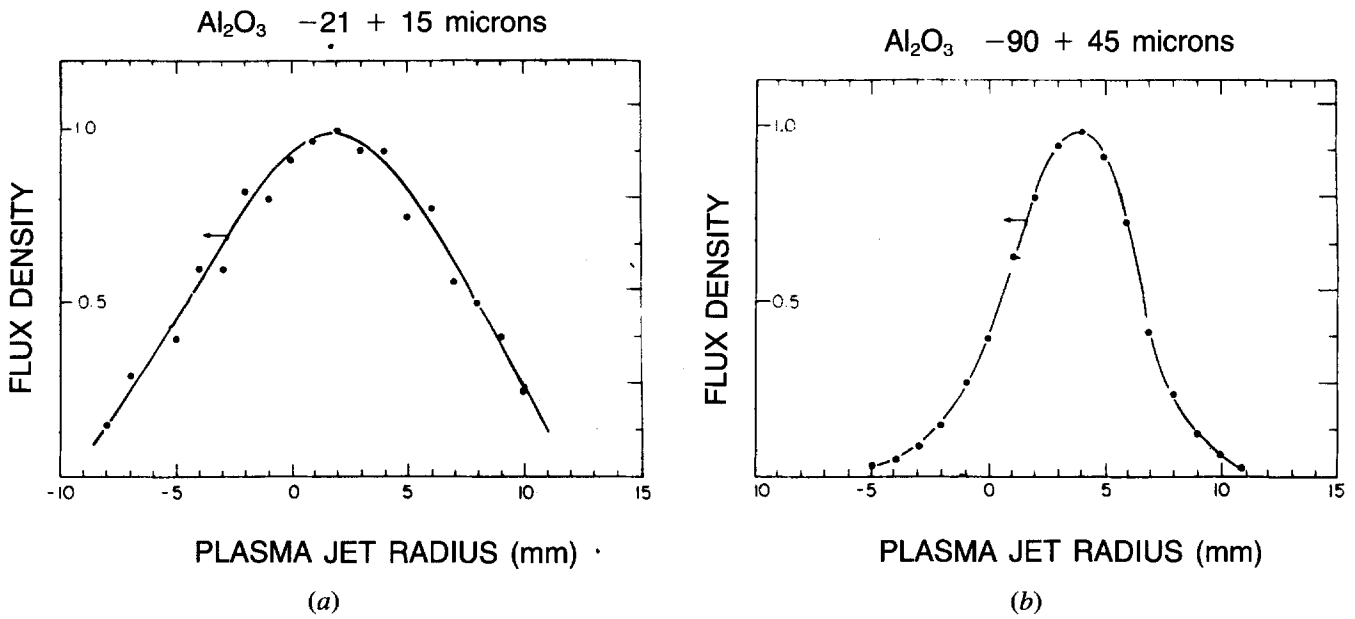

(*a*) (*b*)

Fig. 15—The trajectory distribution (or, more precisely, flux distribution), 75 mm downstream of the nozzle exit, for an Ar-H_2 29 kW plasma jet for alumina particles (*a*) −21 + 15 μm and (*b*) −90 + 45 μm, respectively.

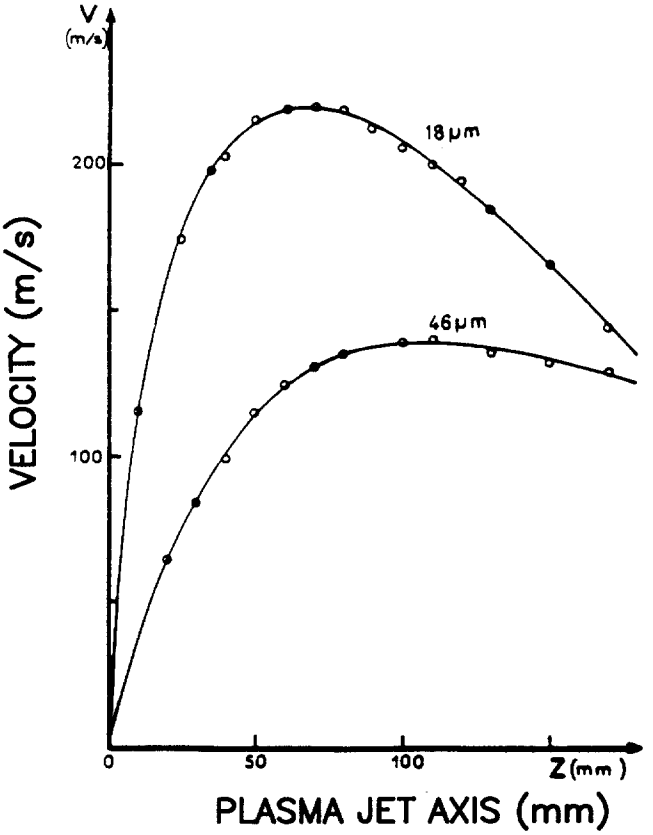

Fig. 16—The evolution along the mean trajectory of the velocity of fused alumina particles with size distributions of −21 + 15 μm and −52 + 40 μm, respectively.[23]

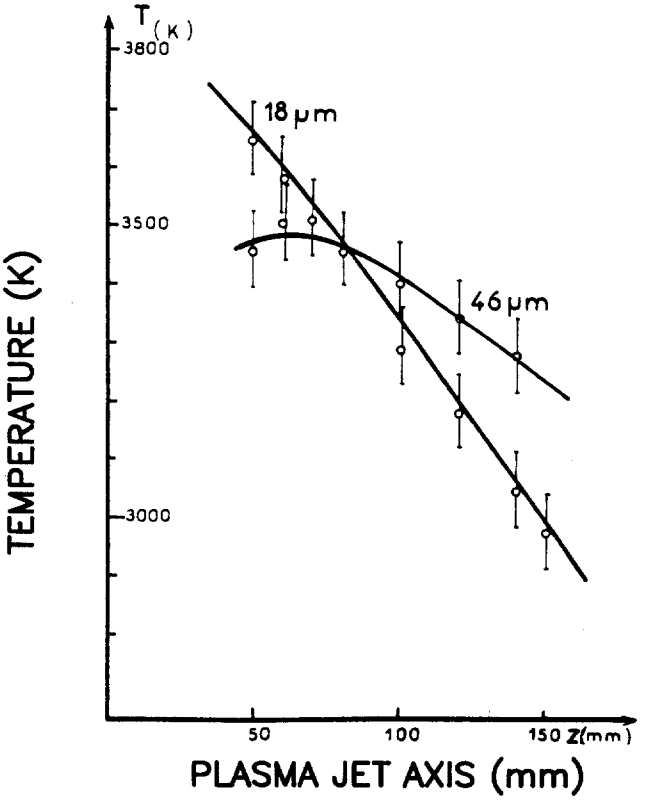

Fig. 17—The evolution along the mean trajectory of the surface temperature of fused alumina particles with size distributions of −21 + 15 μm and −52 + 40 μm, respectively.[23]

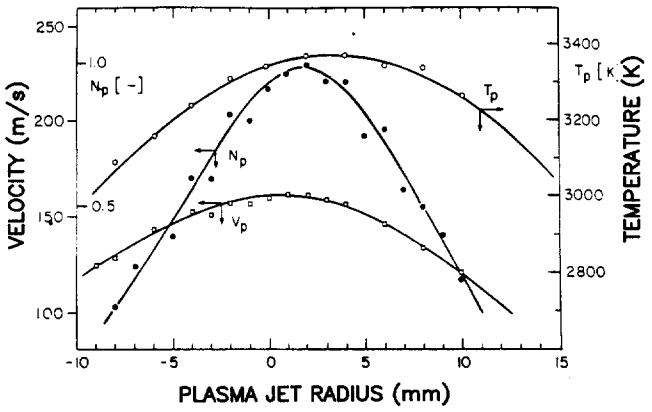

Fig. 18—The particle number flux, velocity, and surface temperature profiles at z = 75 mm in 29 kW Ar-H_2 plasma (45 l/min Ar, 15 l/min H_2).[23]

the velocity, flux, and surface temperature distributions in a plasma jet slice situated 75 mm downstream of the nozzle exit for alumina particles (−21 + 15 μm) injected in a 28 kW Ar-H_2 plasma (45 l/min of Ar, 15 l/min of H_2). As already emphasized in Figure 15(a), the trajectory distribution is broad, as well as are the resulting velocity and surface temperature distributions. With such particles and a substrate located at the same position, the ratio $\alpha/(\alpha + \gamma)$ is 4 pct. This shows that most of the particles are completely molten upon impact. For the 46 μm particles, this ratio is 8 pct, in good correlation with the measurements shown in Figures 16 and 17. With these 46 μm particles, whose surface temperature is lower than that of the 18 μm particles, the heat propagation phenomenon is more important, and all the particles are not necessarily completely molten upon impact. The residence time τ_r of the 18 μm particles along the mean trajectory is about 0.3 ms, time which corresponds to a center temperature of the particle far over melting temperature. For the 46 μm particles, τ_r = 0.7 ms, and with such a residence time, the center temperature is of the order of the melting temperature. However, compared to the 18 μm particles, the less dispersed trajectory distribution of the 46 μm particles probably limits the number of particles traveling in the fringes of the jet where the heat transfer is more reduced. This is illustrated when performing measurements in single pass deposits (whose shape is more or less Gaussian according to the flux distribution shown in Figure 18 and the relative velocity torch-substrate). In the center of the single pass coating (obtained with the 18 μm particles), the ratio $\alpha/(\alpha + \gamma)$ is 3 pct, and it reaches 7 pct in the fringes (the mean value for a complete deposit is 4 pct).

2. *Influence of the power level and plasma gas flowrate*

When increasing the power level, two phenomena occur:

(1) the plasma jet length in air increases (but much less than the power level; see Section IV); and
(2) the plasma velocity increases too; thus, the residence time of the particles decreases.

It is then clear that the increase of the particle temperature will not be proportional to the power level increase. This is illustrated in Figure 19, showing the

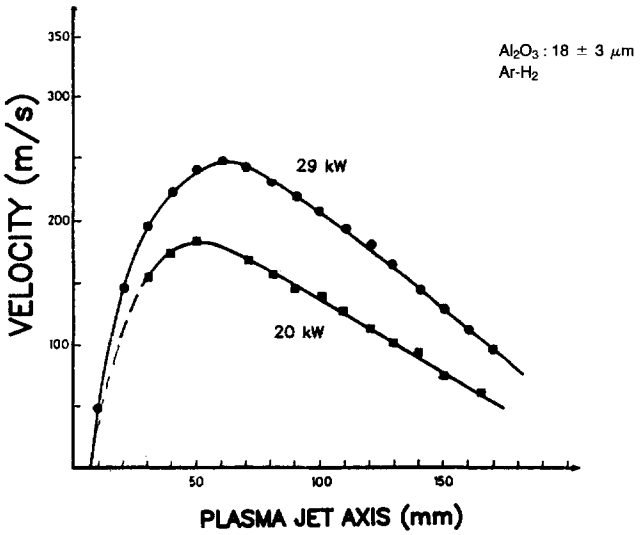

Fig. 19—The influence of the power level on the velocities along the trajectory of alumina particles (−21 + 18 μm) in an Ar-H_2 plasma (45 l/min Ar, 15 l/min H_2).[23]

velocity of alumina particles (−21 + 15 μm) in the Ar-H_2 plasma (45 l/min Ar, 15 l/min H_2) for two power levels: 29 kW (420 A) and 21 kW (280 A). The maximum velocities are 245 m/s and 180 m/s, respectively, and the residence time of the particles in the 29 kW plasma is reduced. Due to the compensation between the two phenomena (reduction of the heat transfer and increase of the energy density), the surface temperature difference between the two power levels is only about 100 K, as illustrated in Figure 20. When treating bigger parti-

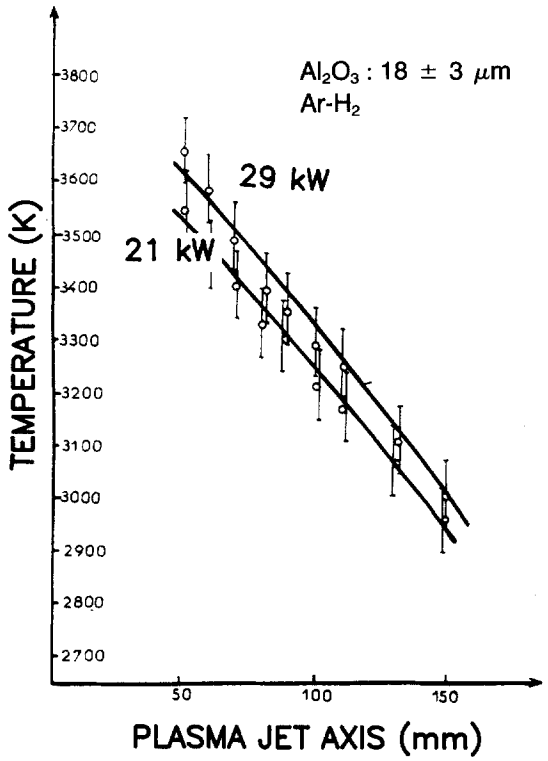

Fig. 20—The influence of the power level on the surface temperature along the trajectory of alumina particles (−21 + 18 μm) in an Ar-H_2 plasma (45 l/min Ar, 15 l/min H_2).[23]

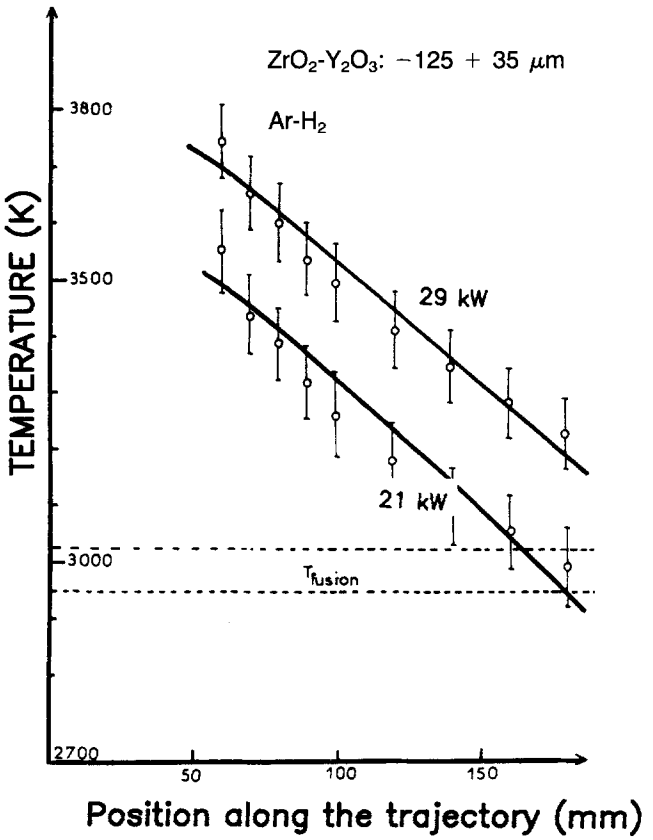

Fig. 21—Influence of the power level on the surface temperature along the trajectory of zirconia particles (stabilized with 8 pct yttria) (−125 + 35 μm) in an Ar-H_2 plasma (45 l/min Ar, 15 l/min H_2).[23]

cles with a broader size distribution, ZrO_2 stabilized with Y_2O_3 (8 wt pct) − 125 + 35 μm, the surface temperature difference between 21 and 29 kW is higher: 250 K (see Figure 21). The close interaction between power level and particle sizes can also be shown in Figure 22, representing the evolution with power level of the density of zirconia coatings for different particle sizes: zirconia

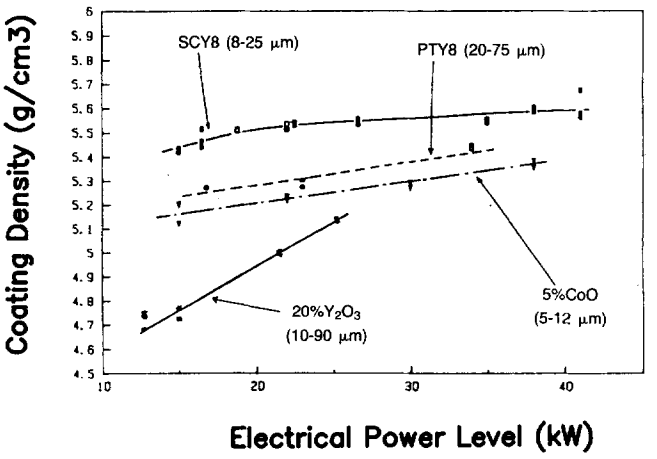

Fig. 22—The influence of the power level (Ar-H_2 plasma: 45 l/min Ar, 15 l/min H_2) on the density of zirconia-sprayed deposits stabilized with yttria (8 wt pct) with size distributions of −25 + 8 μm and −75 + 20 μm, with calcia (10 wt pct) with a size distribution of −12 + 8 μm, or with yttria (20 wt pct) with a size distribution of −90 + 10 μm.[24]

stabilized with yttria (8 wt pct) with size distributions of (−25 + 8 μm) and (−75 + 20 μm), calcia (10 wt pct) (−12 + 5 μm), or with yttria (20 wt pct) (−90 + 10 μm). It is clear that the density increases regularly with the power level corresponding to a better melting of the particles. The best result is obtained with a size distribution of −25 + 8 μm, as could be foreseen from the previous results. The lowest density at high power level obtained with the smallest particles can be explained by the large flux distribution with such particles, the highest surface tension, and the high evaporation rate, especially of calcia, in the central part of the jet. With the biggest particles incompletely molten, the influence of the power level is more drastic.

Another point which must be emphasized is the influence of the plasma gas flowrate. As already mentioned (see Section IV and Figures 11(a) and 11(b)), when increasing the total plasma gas flowrate to 90 l/min (75 l/min Ar, 15 l/min H_2), the constriction of the plasma column increases, thus increasing the power densities and the velocities. These results for the particles are illustrated in Figure 23 where it can be seen (when comparing to Figure 18, obtained with the same particles, the same plasma torch, the same power level but with a total flowrate of 60 l/min) that in spite of a higher velocity (at the maximum 210 m/s against 150 m/s with the lowest flowrate), the surface temperatures are about the same with a better centered flux distribution.

3. *Influence of the powder morphology*

Ceramic particles may be very different even for the same chemical composition and size distribution, depending upon the way they have been manufactured.[35,36] Roughly, they can be classified either in round-shaped particles (agglomerated, agglomerated and calcinated, flame or plasma densified, atomized, *etc.*) or blocky and angular particles (fused and milled or sintered and milled). The round-shaped particles are porous and even hollow while the blocky ones are rather dense. This morphology is very critical for the heat transfer. The fused particles have the coarser shapes, and this seems to play a role in the melting of the particles.[37] The porous particles enhance the heat propagation phenomenon. This can be seen when studying the cross-sections of particles collected in water after their travel in the plasma jet. After plasma treatment, the agglomerated or agglomerated and sintered powders are often hollow spheres (with a rather thin wall) containing unmelted grains.[37] The thickness of the melted wall depends upon the densification of the particles before spraying as well as upon their mean size. For the same size distribution, the melting of the ZrO_2-Y_2O_3 (8 wt pct) particles (−95 + 40 μm) is more uniform for agglomerated particles which have been densified but not at too high a temperature (flame densification). For example, the powder melting is better for agglomerated powders than for agglomerated and sintered powders. The first ones are almost a mixture of monoclinic zirconia and yttria, while the sintered ones are mainly in the tetragonal phase with 20 pct of the monoclinic phase. However, a better melting is obtained with agglomerated flame-densified particles, which are still a mixture of monoclinic zirconia and yttria.[37,38] Similar results have been obtained with nickel-based alloys,[39] and it is worth studying the heat propagation phenomenon inside such agglomerated particles where melting seems to occur along the segregated regions of the original powder. The size of the particles plays a role through the surface tension, which is higher for smaller particles. With big particles, the gas included in the pores will expand and blow up the melted surface as a balloon reducing the heat transfer to the central part of the particle. For zirconia particles (agglomerated and sintered, −105 + 10 μm, stabilized with 8 wt pct yttria), the surface temperature of the particles (for the same power level and plasma gas flowrate) is higher than that of the same particles that have been sintered. Within the shell formed at the surface of the particle, the heated mass is smaller, and thus the temperature is higher. The contrary

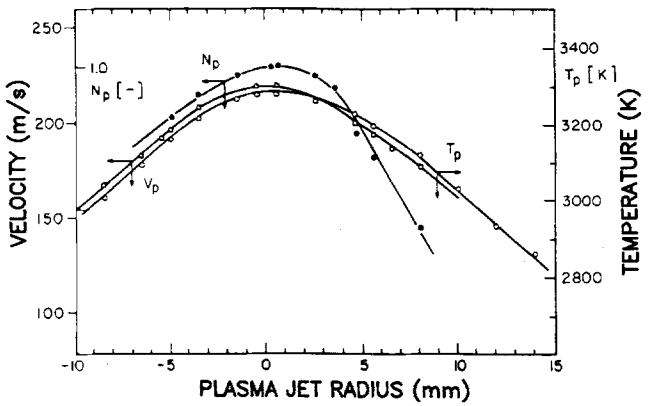

Fig. 23—The particle number flux, velocity, and surface temperature profiles at z = 75 mm in 29 kW Ar-H_2 plasma (75 l/min Ar, 15 l/min H_2).[23]

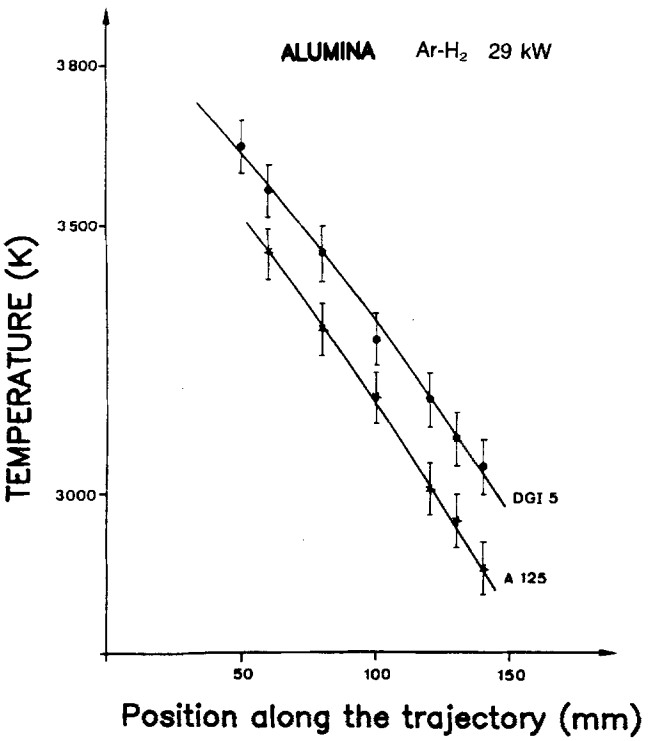

Fig. 24—The surface temperature evolution along the trajectory of two alumina powders fused DGI5 (−21 + 15 μm) and agglomerated (−28 + 10 μm) in a 29 kW Ar-H_2 plasma.[23]

is true for alumina particles (on the one hand, fused ones $-21 + 15$ μm (noted DGI5) and, on the other hand, agglomerated ones ($-28 + 10$ μm) (noted A125)) the surface temperature of the agglomerated ones is a little lower than that of the fused ones (Figure 24). The agglomerated powders, as well as the fused ones, are melted because for both deposits, the ratio $\alpha/(\alpha + \gamma)$ is 2 pct.

VI. CONCLUSIONS

1. Plasma spraying has been used in industry for more than 30 years and is in full development with a sales annual growth rate of 12 pct. It is foreseen that among the sprayed materials, ceramics is of increasing interest, and thus this paper has been devoted to a better understanding of the physical phenomena involved in the momentum, mass, and heat transfers between Ar-H_2 plasma jets flowing in air and oxide particles such as alumina and stabilized zirconia. These transfers have been modeled and measured, and the flux, velocity, and surface temperature distributions of the particles upon impact calculated or measured have been correlated to some coating properties. The coatings were obtained under the same spraying conditions for substrate cooling and relative displacements torch/substrate, avoiding any load effect with ratios of particle to plasma gas mass flowrates lower than 0.1 and adjusting the spraying distance to obtain as many completely molten particles as possible.
2. Calculations of these plasma-particle transfers and measurements of the plasma jet temperatures, of the particle trajectory, velocity, and surface temperature distributions, as well as vapor cloud sizes and densities have shown an acceptable agreement between calculated and measured distributions. However, it must be emphasized that since all measurements are statistical (for n particles passing into the measurement volumes), their present precision does not allow one to choose among the different theories, especially between the coefficients accounting for the steep temperature gradients around the particle, the noncontinuum effect, or the evaporation. In spite of that, the theories give a fairly good idea of the particle behavior under thermal plasma conditions.
3. Of course, it is mandatory to know with a good precision the temperature and velocity isocontours of the plasma jets. The performed emission spectroscopic measurements have shown that the length and diameter of the jets are not simply correlated to the dissipated power level and thermal efficiency of the torch, but they depend on:

   a. a careful design of the cathode, plasma gas injector, arc chamber, and anode-nozzle shapes. For the same gas nature and flowrate, power level, thermal efficiency, and nozzle exit diameter, the length of the plasma jet can be increased by a factor up to 1.5 through an appropriate design.
   b. the surrounding air being pumped very rapidly into the plasma jet and cooling it down very quickly (due to the low dissociation temperature of oxygen). As the pumping rate increases with the arc current and plasma gas flowrate, when increasing the power level by doubling the arc current, the length of the jet is multiplied by only 1.3 to 1.4. The diameter of the jet increases, too, with the arc current and that improves particle penetration into the hot core. Of course, when spraying in an argon atmosphere, the length of the jet is multiplied by 1.5 to 2, compared to the same plasma jet in air, and its diameter is also increased.
   c. an increase of plasma gas total flowrate, which results in a more constricted plasma core with higher temperatures, enthalpies, and velocities. This is confirmed by a good melting of the particles (in spite of higher velocities) and better deposit properties.

The highest velocities are, of course, obtained with the smallest particles; however, for particles below 20 μm in diameter, noncontinuum effects and strong evaporation reduce heat and momentum transfers. The strong evaporation is due to heat propagation phenomenon enhanced by the high heat transfer coefficient of Ar-H_2 plasmas (up to 100,000 $W/m^2 \cdot K$) and the low thermal conductivity of the studied oxides. For the small particles (below about 25 μm), especially those traveling in the central part of the hot core, the evaporation is tremendous. (The vapor cloud which surrounds and travels with the particle can reach 10 to 15 times its diameter.) This reduces the heat transfer drastically and also, according to the coatings properties, the size of the splats and the contacts between them. An optimum size of the particles must be determined for their complete melting. When increasing their diameter from 20 to 50 μm, their residence time is doubled, but their melting time is multiplied by 6 and, for the studied 40 kW plasmas, the oxide particles bigger than 45 to 50 μm are not completely molten upon impact.

A very critical point, emphasized by our calculation and measurements, is the trajectory distribution resulting from the product of the size and injection velocity distributions. For small particles, which require high injection velocities to penetrate into the plasma core, the injection velocity distribution is very large, resulting even in very narrow size distributions in large trajectory distributions. These trajectory distributions are larger than those obtained with big particles (for example, $d = 60$ μm) with broad size distributions. A mean particle size with an adequate size distribution must be chosen to improve the quality of the coatings and limit the differences in particle heat treatment as confirmed by the deposit properties.

Finally, in this paper we have been considering the influence of the particle morphology (fused or sintered and milled, agglomerated, agglomerated and calcinated, *etc.*). The measurements have shown that this problem is rather complex. For example, low density particles, such as agglomerated or agglomerated and calcinated ones do not have the same behavior, depending on their size. The bigger ones (over 40 μm), due to heat propagation phenomenon, have a melted shell blown by the included gas and their central part is not, or poorly, melted, while the smaller ones are rather well melted down to their center, their higher surface tension compensating the molten shell blowing. The degree of melting seems also

to depend on the contacts between the small grains forming the particles, a calcinated particle being better molten than a sintered or agglomerated one. Many studies are still necessary to understand these phenomena better.

REFERENCES

1. N.N. Rykalin and V.V. Kudinov: *Pure and Applied Chemistry*, 1976, vol. 48, p. 229.
2. A. Vardelle, P. Fauchais, and M. Vardelle: *Actualité Chimique*, 1981, vol. 10, p. 69.
3. J.H. Zaat: *Ann. Rev. Mater. Sci.*, 1981, vol. 13, p. 9.
4. D. Apelian: "Rapid solidification by plasma deposition" in *Mat. Res. Soc. Symp. Proc.*, North-Holland, New York, Amsterdam, 1984, vol. 30 (Pb.).
5. P. Fauchais, E. Bourdin, J.F. Coudert, and R. McPherson: in *Plasma Chemistry, Topics in Current Chemistry*, M. Venugopalan and S. Veprek, eds., Springer-Verlag, Berlin, 1983.
6. P. Chagnon and P. Fauchais: *Ceramics Int.*, 1984, vol. 10, p. 119.
7. L. Pawlowski: Thèse de Doctorat d'Etat, University of Limoges, France, June 1985.
8. A.R. Nicoll: *Thermal spray CEI Course on High Temperature Materials and Coatings*, (Pb.) Plasma-Technik AG, Wohlen, Switzerland, 1984.
9. A.H. Dilawari and J. Szekely: *Mat. Res. Soc. Symp. Proc.*, 1987, vol. 98, p. 3.
10. A.H. Dilawari and J. Szekely: *Plasma Chemistry, Plasma Processing*, 1987, vol. 7 (3), p. 317.
11. Y.C. Lee and E. Pfender: *Plasma Chemistry, Plasma Processing*, 1987, vol. 7 (1), p. 1.
12. E. Pfender: *Pure and Applied Chemistry*, 1985, vol. 57 (9), p. 1179.
13. Xi Chen: *ISPC8*, K. Akashi, ed., University of Tokyo, Japan, 1987, vol. 1, p. 4.
14. A. Vardelle: *Thèse de Doctorat d'Etat*, University of Limoges, France, July 1987.
15. A. Vardelle, M. Vardelle, and P. Fauchais: *Plasma Chemistry, Plasma Processing*, 1982, vol. 2 (3), p. 255.
16. M. Vardelle, A. Vardelle, P. Fauchais, and M. Boulos: *A.I.Ch.E.*, 1988, vol. 34 (4), p. 567.
17. E. Bourdin, P. Fauchais, and M.I. Boulos: *Int. J. Heat Mass Transfer*, 1983, vol. 26, p. 519.
18. J.A. Lewis and W.H. Gauvin: *A.I.Ch.E.*, 1973, vol. 19, p. 982.
19. Y.C. Lee, K.C. Hsu, and E. Pfender: *ISPC5*, B. Waldie, ed., Heriot Watt University, Edinburgh, Scotland, 1981, vol. 2, p. 795.
20. P. Fauchais, A. Vardelle, M. Vardelle, J.F. Coudert, and J. Lesinski: *Thin Solid Films*, 1984, vol. 14, p. 303.
21. M. Vardelle, A. Vardelle, P. Fauchais, and M.I. Boulos: *A.I.Ch.E.*, 1983, vol. 29 (2), p. 236.
22. P. Proulx, J. Mostaghimi, and M. Boulos: *ISPC8*, K. Akashi, ed., University of Tokyo, Japan, 1987, vol. 1, p. 13.
23. M. Vardelle: Thèse de Doctorat d'Etat, University of Limoges, France, July 1987.
24. D. Lombard: Thèse de Docteur Ingénieur, ENSCI, Limoges, France, 1985.
25. J.F. Coudert: *Thèse de Doctorat d'Etat*, University of Limoges, France, June 1985.
26. J.F. Coudert, J.M. Baronnet, and P. Fauchais: *ISPC6*, M. Boulos, ed., University of Sherbrook, Canada, 1983, vol. 1, p. 102.
27. J. Mishin, M. Vardelle, J. Lesinski, and P. Fauchais: *J. of Physics E: Scientific Instrument*, 1987, vol. 20, p. 620.
28. P. Fauchais, J.F. Coudert, M. Vardelle, A. Vardelle, and C. Trassy: *Mat. Res. Soc. Symp. Proc.*, 1987, vol. 98, p. 101.
29. M. Vardelle, A. Vardelle, P. Fauchais, and C. Trassy: *ISPC8*, K. Akashi, ed., University of Tokyo, Japan, 1987, vol. 1, p. 404.
30. Ph. Roumilhac, J.F. Coudert, J.M. Leger, A. Grimaud, and P. Fauchais: *ISPC8*, K. Akashi, ed., University of Tokyo, Japan, 1987, vol. 1, p. 419.
31. M. Vardelle, A. Vardelle, and P. Fauchais: *Advances in Thermal Spraying*, Pergamon Press, New York, NY, 1986, p. 379.
32. J. Guyonnet: CNRS Patents 124 111, 168044, 1968, and 7044678, 1970, France.
33. P. Fauchais, J.F. Coudert, A. Vardelle, M. Vardelle, A. Grimaud, and Ph. Roumilhac: *Proc. NTSC 87*, Orlando, FL, AIME, 1988, p. 11.
34. M. Brossa and E. Pfender: *Plasma Chemistry, Plasma Processing*, 1988, vol. 8 (1), p. 75.
35. G. Schweir: in *Advances in Thermal Spraying*, Pergamon Press, New York, NY, 1986, p. 277.
36. B. Krismer: *Proc. MRS Europe*, Editions de Physique, Paris, Nov. 1985, p. 33.
37. F. Gitzhofer: *Thèse de l'Université de Limoges*, Limoges, France, May 1988.
38. D. Bernard, F. Gitzhofer, P. Fauchais, and M. Martin: *1st Plasma Technik Symp.*, (Pb.) Plasma Technik, Wohlen, Switzerland, 1988, vol. 2, p. 143.
39. R.W. Smith and D. Apelian: *Mat. Res. Soc. Symp. Proc.*, 1987, vol. 98, p. 89.